Nano Energy 126 (2024) 109710

Contents lists available at ScienceDirect

Nano Energy

journal homepage: www.elsevier.com/locate/nanoen

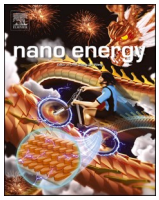

Electrolyte design for zinc dynamic windows with fast switching that cycle more than 11,000 times with high optical contrast

Nikhil C. Bhoumik, Samantha M. Thompson, Christopher J. Barile *

Department of Chemistry, University of Nevada, Reno, Nevada 89557, United States

ARTICLE INFO

Keywords:
Dynamic windows
Smart windows
Reversible metal electrodeposition (RME)
Zinc electrodeposition
Transparent conducting electrodes

ABSTRACT

The widespread adoption of electronically adjustable dynamic windows promises to significantly improve the energy efficiency of buildings. In this manuscript, we develop robust dynamic windows based on the reversible metal electrodeposition (RME) of Zn from DMSO electrolytes. We systematically interrogate the role of anions, cations, and polymer additives on electrolyte properties and develop design rules to increase the electrochemical and optical reversibility of these systems. This fundamental understanding allows us to develop an electrolyte that facilitates reversible Zn electrodeposition with unprecedented speed and reversibility with a Coulombic efficiency of 99.5%. We implement this electrolyte into practical two-electrode 25 cm^2 dynamic windows and demonstrate that these devices switch more than 11,000 times without degradation in optical performance and without altering the switching speed or voltage profile. This outstanding durability is unprecedented in the field of RME windows and brings metal-based dynamic windows substantially closer to successful commercialization.

1. Introduction

Dynamic windows are electronically modulated films that mitigate heat and light transference through the utilization of varying degrees of optical transparency. These devices are important for increasing the energy efficiency in buildings, which are responsible for 40% of energy consumption in the United States [1]. Dynamic windows result in an average of 10–20% energy savings in buildings compared to traditional static windows due to increased energy efficiency associated with lighting, heating, and cooling [2].

Three well-established categories of electronically-controlled dynamic windows are electrochromic windows, suspended particle devices, and liquid crystal devices. While each technology has its own advantages and disadvantages, electrochromic windows, which contain materials whose transmission changes with applied voltage, are the most widely studied and commercialized [3]. A variety of electrochromic materials have been explored including transition metal oxides [4], polymers [5], nanoparticles [6], and redox-active molecules [7],. Despite copious research devoted to electrochromic materials, electrochromic windows do not simultaneously possess the fast switching times, color neutral switching, excellent durability, and low cost needed to achieve widespread implementation [4].

In addition to these three well-established categories of electronically-controlled dynamic windows, a less-explored method of constructing dynamic windows utilizes reversible metal electrodeposition (RME). In RME windows, a transparent electrode, typically tin-doped indium oxide (ITO) on glass, is immersed in an electrolyte solution containing metal ions. Upon application of a cathodic voltage, the metal ions in the solution deposit onto the ITO, resulting in a darkening of the glass [7–9]. This reduction is charge balanced by concomitant oxidation on the counter electrode, which in most embodiments consists of metal mesh. To switch the device back to its clear state, the polarity of the applied voltage is reversed such that the metal on the transparent working electrode is oxidized back to metal ions in the electrolyte and metal is replated on the counter electrode.

The use of metals in RME windows has several benefits over other dynamic window technologies. Many metals inherently exhibit traits that support robust and aesthetically-pleasing devices such as photostability, inertness towards non-electrochemical reactions, black coloration, and high opacity [8]. Specifically, metals are almost completely opaque at thicknesses of only 20–30 nm as compared to most electrochromic materials, which require several hundred nanometers of material to achieve comparable opacity levels [10]. The high opacity of metals allows them to switch quickly and with a very large optical dynamic range.

The careful selection of metals plays a pivotal role in the design of

* Corresponding author.
E-mail address: cbarile@unr.edu (C.J. Barile).

https://doi.org/10.1016/j.nanoen.2024.109710
Received 21 March 2024; Received in revised form 1 May 2024; Accepted 5 May 2024
Available online 9 May 2024

robust RME windows. A multitude of metals have been previously explored in aqueous RME electrolytes including Cu, Au, Ag, and Bi [9]. Cu and Au are both highly colored in their metallic state (oxidation state of zero), rendering them unsuitable for most applications. The red color of Cu can be obviated by including Bi^{3+} ions into the electrolyte to allow for the formation of black Bi-Cu electrodeposits that possess acceptable color [11]. Unfortunately, Bi^{3+} ions are typically only soluble under highly acidic conditions that result in the etching of the ITO working electrode [11]. Another problem with Cu-based electrolytes is the blue color of Cu^{2+} electrolytes, which can limit initial device transparency. However, this problem can be overcome if the electrolyte in the device is thin such that the electrolyte transmission remains high [12]. Zn has recently emerged as an intriguing metal for RME windows due to the colorless nature of Zn^{2+} ions and the propensity for Zn to form highly compact electrodeposits.

Aqueous Zn electrolytes, however, are thermodynamically unstable with respect to the H_2 evolution reaction because the standard reduction potential of Zn/Zn^{2+} is −0.76 V vs. SHE. Previous research has shown that although H_2 generation can be kinetically passivated on ITO electrodes, an insulating film of $Zn(OH)_2$ and/or ZnO slowly accumulates on the electrodes, which hinders device cycle life [13]. To avoid the formation of these deleterious side products, we recently investigated Zn RME dynamic windows in DMSO, a polar aprotic solvent, and showed that these electrolytes support devices with excellent durability, color-neutral switching, and high opacity [14]. This choice of solvent is crucial in RME dynamic window applications because polar aprotic solvents inhibit H_2 generation and limit the formation of insulating side products such as $Zn(OH)_2$, enabling enhanced cycling performance of the devices. DMSO also possesses a wide electrochemical potential window and dissolves a variety of Zn and supporting ion salts [15].

Despite clear advantages of Zn DMSO electrolytes, whether or not the device durability needed for practical dynamic windows can be achieved is an outstanding question. If a dynamic window is cycled a few times every day for 20–30 years, the device will need to last around 50,000 cycles. For this reason, ASTM-E2141 standards for dynamic windows stipulate 50,000 cycles without substantial degradation [16]. There are no existing reports of RME windows that exhibit this level of cycling durability, and previous attempts have only achieved around 10,000 cycles using complex variable voltage profiles [14]. Optimizing cycling speed is also ideal, though not specifically outlined by ASTM standards, so as to decrease time involved per cycle and satisfy consumer requirements.

In this paper, we investigate the role of various anions in Zn DMSO electrolytes in an attempt to improve cyclability and switching speeds of RME dynamic windows. Previous Zn battery research indicates that the incorporation of supporting ions significantly impacts the morphology of the Zn electrodeposition through alterations of the Zn coordination complexes and electrodeposit growth rate [17]. These properties are correlated to switching speed as more consistent and even deposition rates blocks light with a higher efficiency than less uniform electrodeposits. Through systematic electrolyte design, we develop Zn DMSO electrolytes with lithium trifluoroacetate ($LiCF_3COO$) and lithium formate (LiCOOH) that enable reversible Zn electrodeposition with an impressive 99.5% coulombic efficiency. This formulation produces encouraging results, showcasing an improved switching speed and optical contrast ratio compared to previously reported Zn DMSO electrolytes [14]. Our investigation extends to practical two-electrode dynamic windows, in which we demonstrate devices that switch 14,000 cycles without compromising optical contrast or switching speed, positioning them as promising contenders for future commercial applications.

2. Results and discussion

2.1. Three-electrode studies for designing high-performance zinc electrolytes

In our previous study, we designed a Zn DMSO electrolyte consisting of 300 mM $ZnBr_2$, 300 mM $Zn(CH_3COO)_2$, and 400 mM $NaCH_3COO$ that allows for optically and electrochemically reversible Zn electrodeposition. In particular, this electrolyte enables 25 cm^2 devices to cycle about 10,000 times without any decline in optical contrast [14]. More specifically, cycles consisting of a 30 s darkening time and a 60 s lightening time allow the window to switch between a 75% transmission clear state and a 30% transmission dark state for about 10,000 cycles. However, to maintain a constant contrast ratio and switching speed, the magnitude of voltage applied during electrodeposition was slowly increased during cycling. In other words, a progressively greater driving force for electrodeposition was needed to maintain the same optical properties of the device, indicating that cycling slowly degrades the device. Indeed, after 10,000 cycles, we detected the formation of acetic acid within the electrolyte, as evidenced by ^1H NMR spectroscopy, which presumably forms from the reaction of acetate with adventitious water in the DMSO electrolyte [14]. We hypothesize that the formed acetic acid impedes long-term device cyclability, given its ability to etch ITO. The generation of H_2 bubbles is also observed during long-term cycling when voltages more negative than −0.9 V are employed for device darkening, and this undesired H_2 evolution may also originate from the formed acetic acid.

In an attempt to overcome these challenges, we have replaced the acetate salts in the electrolyte with $LiCF_3COO$ and LiCOOH, in addition to systematically exploring related derivatives. Trifluroacetic acid and formic acid have pK_a values of 0.52 and 3.75, respectively, making them stronger acids than acetic acid, which has a pK_a of 4.76 [18–20]. As a result, the trifluroacetate and formate anions are more stable and less likely to become protonated to their corresponding acids during device cycling. In this manner, we envision that the utilization of $LiCF_3COO$ and LiCOOH might improve the performance of Zn RME windows. Specifically, formate in aqueous Zn electrolytes has been shown to facilitate electrodeposit stripping [17]. The use of trifluroacetate can accelerate Zn electrodeposition, but previous attempts at Zn electrolytes using trifluroacetate without formate resulted in poor Coulombic efficiency due to incomplete stripping [13]. We therefore elected to investigate electrolytes with both trifluroacetate and formate to achieve fast electrodeposition and stripping kinetics.

Cyclic voltammograms (CVs) coupled with transmission measurements are commonly employed as a first step in RME electrolyte design [21]. This approach allows for the study of electrochemical reactions during cycling, facilitating the optimization of electrolytic formulations to achieve high-quality films with desirable optical properties and reversibility. Fig. 1a, red line, displays a CV of Zn electrodeposition and stripping on a Pt-coated ITO (Pt-ITO) working electrode with an electrolyte containing 300 mM $ZnBr_2$, 200 mM $LiCF_3COO$, and 400 mM LiCOOH in DMSO, which is denoted in this work as the Li-ZnDMSO electrolyte. The ITO working electrode is modified with Pt nanoparticles to improve metal electrodeposition uniformity as has been described previously [22,23]. During the initial negative voltage going sweep, cathodic current initiates Zn electrodeposition at an onset potential of −0.30 V vs. Zn/Zn^{2+} for the Li-ZnDMSO electrolyte, which is more positive than the electrolyte containing only 300 mM $ZnBr_2$ (-0.41 V vs Zn/Zn^{2+}, Fig. 1a, black line). However, with the introduction of 2 wt% polyvinyl alcohol (PVA) in this electrolyte, the onset potential shifts more positively to −0.26 V vs. Zn/Zn^{2+} (Fig. 1, blue line) similar to the onset potential of the previously studied ZnDMSO electrolyte [14]. PVA has been previously employed as an electrolyte additive to improve the uniformity of metal electrodeposits [22]. The lower deposition onset potential with PVA indicates a reduced overpotential for Zn electrodeposition in the presence of PVA. The shape of the negative-going reductive sweep varies with electrolyte composition. In

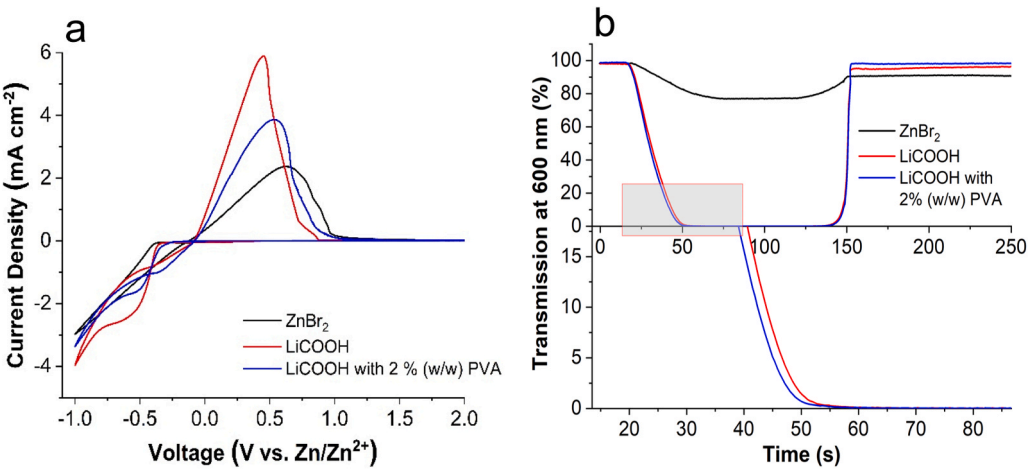

Fig. 1. Spectroelectrochemistry of Pt-Modified ITO Electrodes in DMSO Electrolytes with Various Compositions. Cyclic voltammograms (a) and corresponding transmission at 600 nm (b) of Pt-modified ITO electrodes at a scan rate of 20 mV s^{-1} in DMSO electrolytes containing 300 mM $ZnBr_2$ (black line), 300 mM $ZnBr_2$, 200 mM $LiCF_3COO$, and 400 mM LiCOOH (red line), and 300 mM $ZnBr_2$, 200 mM $LiCF_3COO$, 400 mM LiCOOH (blue line), and 2 wt% PVA.

particular, the two Li-ZnDMSO electrolytes contain a diffusion-limited Zn electrodeposition peak, while the electrolyte containing only $ZnBr_2$ does not exhibit this peak. This difference likely arises from the differences in the coordination complexes present in the various electrolytes. Specifically, the formate anion is expected to bind to Zn^{2+}, potentially decreasing the diffusion coefficient of the coordination complex, which gives rise to a diffusion-limited peak. In contrast, the coordination complexes for the electrolyte with only $ZnBr_2$ are much smaller, giving rise to a higher diffusion coefficient that eliminates the presence of a peak within the voltage range scanned during the CV. The diffusion coefficients of coordination complexes also vary with electrolyte viscosity, which is impacted by PVA. CVs for a wide of range of electrolyte compositions are reported in this manuscript, and these factors result in the various reductive peak shapes observed.

During the positive-going sweep, anodic stripping peaks corresponding to the dissolution of the deposited Zn back to Zn^{2+} are observed for all three electrolytes. The Coulombic efficiencies, calculated as the ratio of the integrated anodic charge to the integrated cathodic charge in the CVs, are 99.0% and 99.5% for the Li-ZnDMSO electrolytes without and with PVA, respectively, which indicate that both electrolytes exhibit excellent electrochemical reversibility. The corresponding transmissions of the electrodes decrease to below 0.1% as

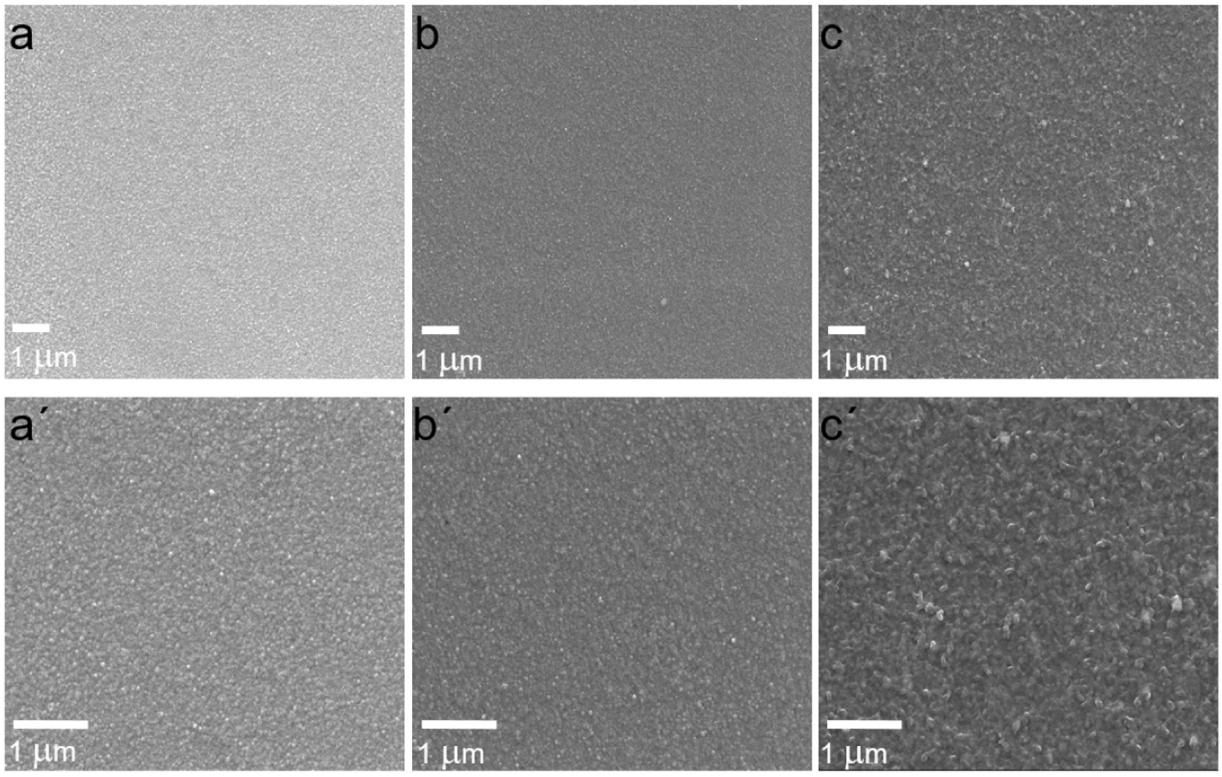

Fig. 2. Impact of PVA Concentration on Zn Electrodeposit Morphology. Scanning electron micrographs of Zn electrodeposits produced from the Li-ZnDMSO electrolytes containing 300 mM $ZnBr_2$, 200 mM $LiCF_3COO$, and 400 mM LiCOOH without PVA and using chronoamperometry at −0.9 V until electrode transmission is equal to 5% (a, a′, two different magnifications). Electrodeposits were produced using analogous conditions with 2 wt% PVA with an electrode transmission of 5% (b, b′, two different magnifications) and 0.1% (c, c′, two different magnifications).

metal deposition occurs and then return to near their original values after the metal is stripped off (Fig. 1b). However, for the electrode using the Li-ZnDMSO electrolyte with PVA, the electrode reaches 1% transmission about 2 s more quickly than the electrode without PVA and also exhibits slightly greater optical reversibility. The faster darkening speed in the presence of PVA suggests that PVA enhances the compactness of the Zn electrodeposits on the ITO, which causes them to block light more efficiently. Indeed, significantly less charge is passed during the chronoamperometry used to produce the electrodeposits with 5% transmission for the electrolyte with PVA (10 mC cm^{-2}) than without PVA (15 mC cm^{-2}), which indicates that electrodeposits from the PVA-containing electrolyte are more compact. This finding is further corroborated by SEM imaging (Fig. 2 and Fig. S1) and aligns with the observations of Strand et al. for a Bi-Cu RME electrolyte with PVA [22]. Additionally, recent studies have highlighted that light absorption varies significantly as a function of the morphology of metal electrodeposits [24,25].

In an attempt to elucidate the influence of the trifluoroacetate anion in the Li-ZnDMSO electrolytes, we increased the concentration of $LiCF_3COO$ from 200 mM to 300 mM. The electrode with the increased $LiCF_3COO$ concentration exhibits significantly decreased optical contrast despite nearly similar anodic and cathodic peak current densities (Fig. S2). SEM imaging reveals a rougher surface consisting of larger particles (Fig. S3) compared to the smooth, compact electrodeposits obtained from the other Li-ZnDMSO electrolytes (Fig. 2). Although the mechanism explaining why a greater trifluoroacetate concentration results in rough electrodeposits is unclear, it may be related to trifluoroacetate adsorption on the electrode or alteration of the identity of Zn coordination complexes in the electrolyte. We also examined the analogous electrolyte with 100 mM $LiCF_3COO$, which exhibits inferior spectroelectrochemical properties to the electrolyte with 200 mM $LiCF_3COO$ (Fig. S2). Due to the superior spectroelectrochemical properties of the Li-ZnDMSO electrolyte containing 200 mM $LiCF_3COO$, we focus the remainder of this manuscript on this electrolyte and related derivatives.

2.2. Impact of halides and formate ions on the performance of Li-ZnDMSO electrolytes

To understand the role of alkali metal formate anion on the performance of Li-ZnDMSO electrolytes, we systemically varied the formate salts, namely LiCOOH, NaCOOH, and KCOOH. The CVs for all three Zn electrolytes containing formate anions exhibit similar maximum cathodic current densities (Fig. 3a). In contrast, the peak anodic current densities during Zn stripping vary significantly across the electrolytes, which results in the Coulombic efficiencies varying in the order of Li^+ (99.0%) > Na^+ (80.6%) > K^+ (66.7%). This sequencing of the Coulombic efficiencies matches that of the optical reversibility demonstrated by the electrodes, in which smaller alkali metal ions exhibit better optical reversibility (Fig. 3b). This result is expected because electrolytes with higher Coulombic efficiencies facilitate Zn stripping, which also promotes good optical reversibility. Electrolyte conductivity measurements reveal that electrolyte conductivity also increases in the order of $Li^+ > Na^+ > K^+$ (Table S1), suggesting that ion pairing, which is the aggregation of charged species in solution, is minimized in the LiCOOH electrolyte. With less ion pairing, disassociated formate ($COOH^-$) is expected to be more predominant in the LiCOOH electrolyte. In previously studied aqueous Zn RME electrolytes, formate plays a crucial role in enhancing Zn stripping kinetics [17]. Thus, we hypothesize that the LiCOOH electrolyte exhibits enhanced Coulombic efficiency and optical reversibility compared to the analogous NaCOOH and KCOOH electrolytes due to the greater stability of disassociated formate in the LiCOOH electrolyte, which enhances Zn stripping kinetics.

While designing Li-ZnDMSO electrolytes, we also assessed the effect of lithium halide compositions on Zn electrodeposition and stripping dynamics. We substituted the 400 mM LiCOOH component of the Li-ZnDMSO electrolyte with different halide salts at the same concentration and performed spectroelectrochemistry (Fig. 4). Of the electrolytes in this series, the LiF electrolyte resulted in the lowest current density and least optical reversibility (Fig. 4, purple line), likely due to the formation of insoluble and insulating fluorides on the electrode surface such as ZnF_2. Furthermore, the LiI electrolyte is not suitable for RME devices because of its dark yellow color, which explains the low initial transmission of 56% (Fig. 4b, red line). The CVs of the LiBr (Fig. 4a, blue line) and LiCl (Fig. 4a, green line) electrolytes possess high magnitude deposition current densities. In terms of optical performance, the LiBr electrolyte facilitates a higher optical contrast than the LiCl electrolyte (Fig. 4b). Bromide is known to accelerate metal electrodeposition and alter electrodeposition morphology [26,27] that evidently, in this case, improves the light-blocking ability of the film. Crucially though, both the Coulombic efficiency and the optical reversibility of the LiBr and LiCl electrolytes are inferior to those of the LiCOOH electrolyte (Table S1). These results indicate that formate is key for facilitating optically reversibility Zn RME systems in DMSO.

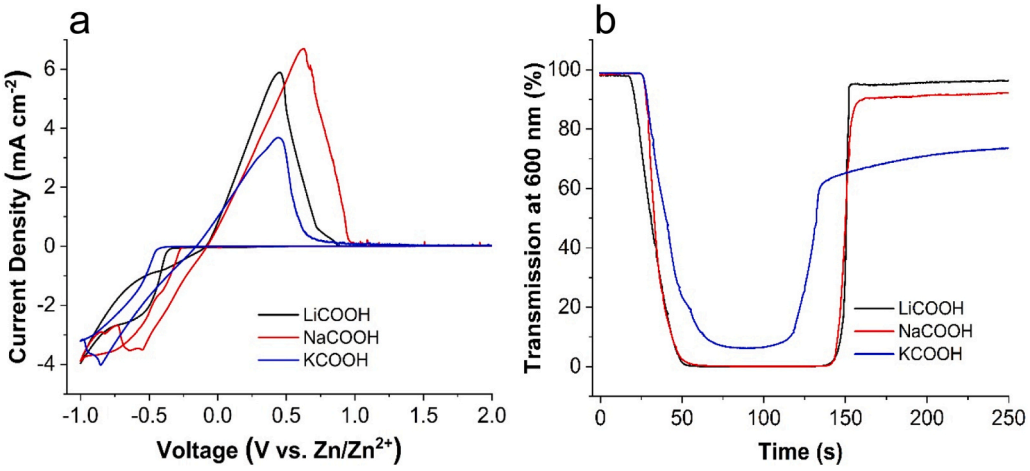

Fig. 3. Impact of Formate Salt Variations in DMSO Electrolytes on Spectroelectrochemistry of Pt-Modified ITO Electrodes. Cyclic voltammograms (a) and corresponding transmission at 600 nm (b) of Pt-modified ITO electrodes at a scan rate of 20 mV s^{-1} in DMSO electrolytes containing 300 mM $ZnBr_2$ and 200 mM $LiCF_3COO$ with 400 mM LiCOOH (black line), 400 mM NaCOOH (blue line), or 400 mM KCOOH (red line).

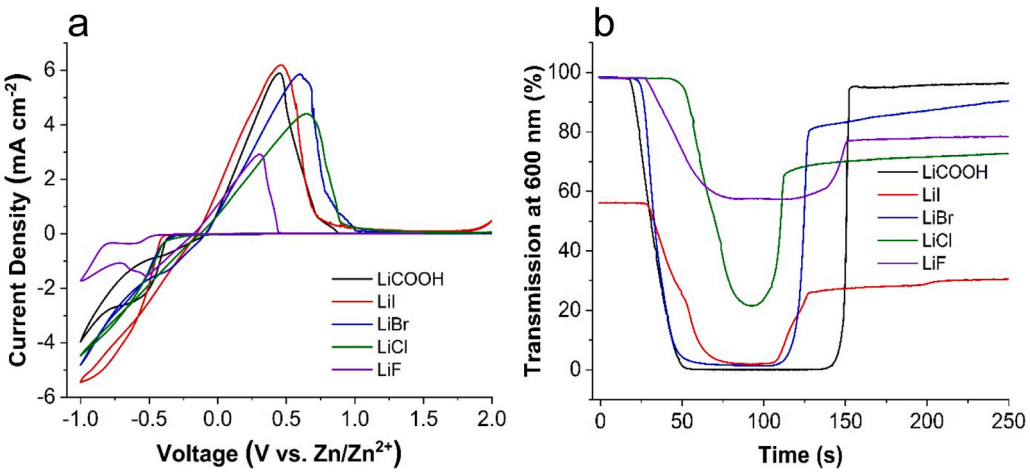

Fig. 4. Influence of Different LiX (X = COOH, I, Br, Cl, F) Salts on Spectroelectrochemistry of Pt-Modified ITO Electrodes. Cyclic voltammograms (a) and corresponding transmission at 600 nm (b) of Pt-modified ITO electrodes at a scan rate of 20 mV s^{-1} in DMSO electrolytes containing 300 mM $ZnBr_2$ and 200 mM $LiCF_3COO$ with 400 mM LiCOOH (black line), 400 mM LiI (red line), 400 mM LiBr (blue line), 400 mM LiCl (green line), or 400 mM LiF (purple line).

2.3. Influence of acetates and haloacetate anions on designing Li-ZnDMSO electrolytes

To understand further the spectroelectrochemical behavior of formate in the Li-ZnDMSO electrolyte, we systematically substituted LiCOOH for different alkali acetate salts while keeping the other electrolyte components the same. Like the three alkali metal formate electrolytes (Fig. 3), the same trend of $Li^+ > Na^+ > K^+$ for the three acetate electrolytes holds for Coulombic efficiency, optical reversibility, and electrolyte conductivity (Table S1). In a manner analogous to formate, these results suggest a greater stability of disassociated acetate anion as the alkali metal cation size decreases, which results in increased spectroelectrochemical reversibility. Furthermore, the $LiCH_3COO$ electrolyte is slightly inferior to the LiCOOH electrolyte in terms of optical contrast (Fig. 5b, red line vs. black line), Coulombic efficiency, and optical reversibility (Table S1). This result suggests that formate more readily facilitates Zn stripping than acetate, a finding that matches previous studies with aqueous Zn RME electrolytes and was ascribed to the less sterically encumbered nature of formate [17].

We also systematically substituted the 200 mM $LiCF_3COO$ electrolyte component with other haloacetates of the same concentration and performed spectroelectrochemical measurements (Fig. 6). Additionally, we tested electrolytes containing $LiCF_3SO_3$, $LiPF_6$, or $LiClO_4$ (Fig. S4). Although the Zn electrolytes with the aforementioned substituents exhibit a consistent deposition onset potential and share general Zn deposition and stripping characteristics with the trifluoroacetate electrolyte, there are distinguishable differences observed in their Coulombic efficiencies and optical reversibilities (Table S1). Although some of the electrolytes exhibit promising optical reversibility, all of these electrolyte derivatives exhibit significantly lower Coulombic efficiencies compared to the 99.0% value measured for the trifluoroacetate electrolyte (Li-ZnDMSO). These results emphasize the important synergy between the three electrolyte components in the Li-ZnDMSO electrolyte that ensure high optical and electrochemical reversibility for Zn RME.

2.4. Effect of viscosity on Zn RME electrolytes

It is advantageous for practical RME windows to contain viscous electrolytes to facilitate electrolyte dispensing during manufacturing. Additionally, viscous electrolytes are preferred from a safety standpoint as the electrolyte will not flow as readily if the window breaks. Electrolyte viscosity can be increased with polymers such as hydroxyethylcellulose (HEC) and PVA [28]. Because more viscous electrolytes decrease ionic conductivity, metal electrodeposition kinetics are also typically reduced [29]. However, polymers including both HEC and PVA

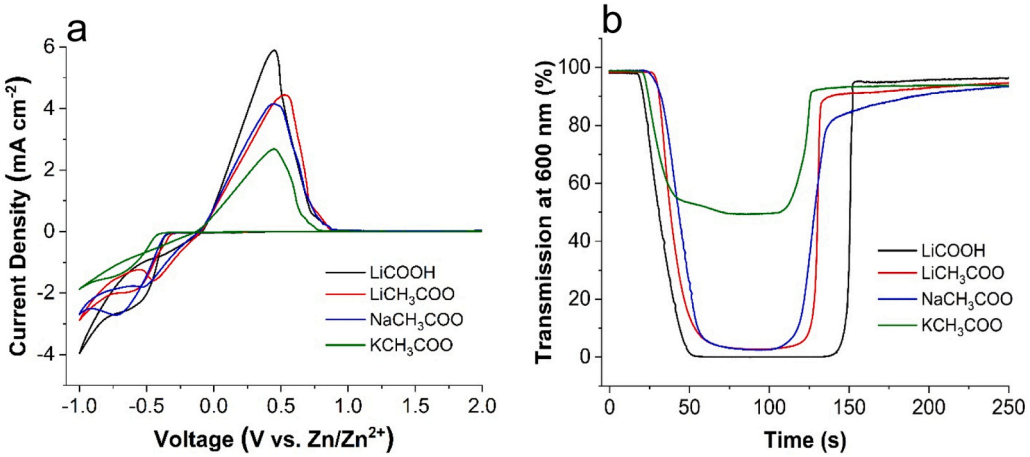

Fig. 5. Impact of Acetate Salt Variation in DMSO Electrolytes on Spectroelectrochemistry of Pt-Modified ITO Electrodes. Cyclic voltammograms (a) and corresponding transmission at 600 nm (b) of Pt-modified ITO electrodes at a scan rate of 20 mV s^{-1} in DMSO electrolytes containing 300 mM $ZnBr_2$ and 200 mM $LiCF_3COO$ with 400 mM LiCOOH (black line), 400 mM $LiCH_3COO$ (red line), 400 mM $NaCH_3COO$ (blue line), or 400 mM KCH_3COO (green line).

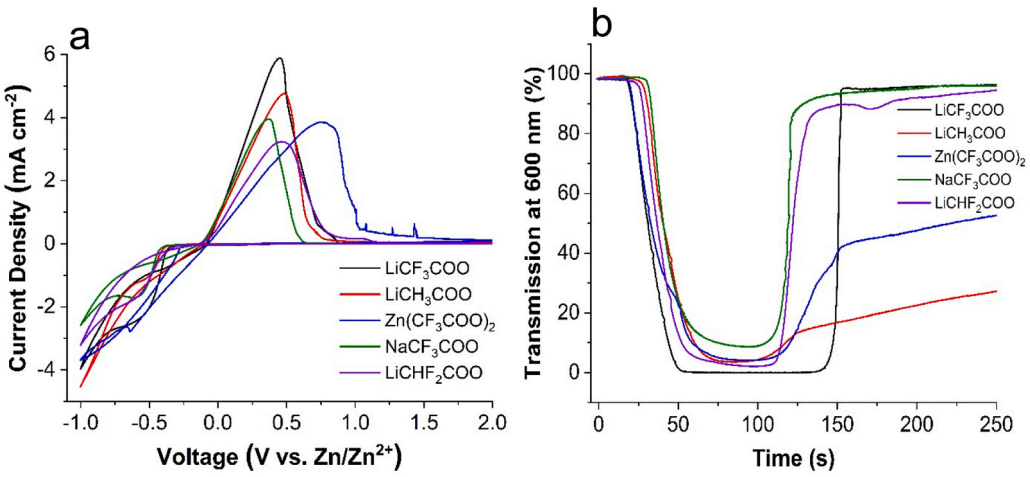

Fig. 6. Influence of Trifluoroacetate Carboxylate Salt Variation in DMSO Electrolytes on Spectroelectrochemistry of Pt-Modified ITO Electrodes. Cyclic voltammograms (a) and corresponding transmission at 600 nm (b) of Pt-modified ITO electrodes at a scan rate of 20 mV s^{-1} in DMSO electrolytes containing 300 mM $ZnBr_2$ and 400 mM LiCOOH with 200 mM $LiCF_3COO$ (black line), 200 mM $LiCH_3COO$ (red line), 200 mM $Zn(CF_3COO)_2$ (blue line), 200 mM $NaCF_3COO$ (green line), or 200 mM $LiCHF_2COO$ (purple line).

can favorably alter the morphology of metal electrodeposits, which causes them to block light more efficiently [9,28]. Often times, this beneficial impact on morphology outweighs the negative impact of diminished electrodeposition kinetics such that the overall switching speed of RME electrolytes with polymer additives is improved.

Without PVA, the Li-ZnDMSO electrolyte has a viscosity of 2.0 cP. As expected, the viscosity of the electrolyte increases with increasing PVA concentration. Specifically, the viscosities of the 2 wt%, 5 wt%, and 10 wt% Li-ZnDMSO electrolytes are 200 cP, 260 cP, and 360 cP, respectively. Furthermore, increasing electrolyte viscosity decreases electrolyte conductivity (Table S1).

The spectroelectrochemical data in Fig. 7 reflects the interplay between improved electrodeposit morphology and decreased RME kinetics. Specifically, the electrolyte with 2 wt% PVA exhibits improved optical reversibility and Coulombic efficiency compared to the electrolyte without PVA despite the lower magnitude of current density observed in the CV. The beneficial impact of the addition of 2 wt% PVA in the Li-ZnDMSO electrolyte was previously discussed in Section 2.1 (Fig. 1). Here, we also point out that higher concentrations of PVA (5 wt % and 10 wt%) impede the optical reversibility of Zn RME (Fig. 7b, red and green lines). Interestingly, the deposition onset potential for Zn electrodeposition for the CVs of the electrolytes varies in the order of 5% PVA > 2% PVA ~ 10% PVA > 0% PVA. These data indicate that there is a complex relationship between PVA concentration and Zn electrodeposition dynamics likely due to competing factors of changing morphology of the electrodeposition and changing reaction kinetics. Another example of the complexity that arises from these competing factors is that the tinting speed of the electrolyte containing 10% PVA is faster than the electrolyte with 5% PVA.

2.5. *Practical two-electrodes 25 cm^2 dynamic windows and cyclability*

Having established the excellent spectroelectrochemical reversibility of the Li-ZnDMSO electrolyte with 2 wt% PVA, we next discuss the implementation of this electrolyte into practical two-electrode 25 cm^2 dynamic window prototypes. These prototypes utilize aesthetically-pleasing Zn meshes with grid lines that are (31.5 ± 0.8) μm thick [13]. Applying a voltage of −0.9 V for 60 s to a 25 cm^2 device decreases its transmission from approximately 85% to less than 0.1% across the visible portion of the electromagnetic spectrum (Fig. 8a). The device also displays excellent optical contrast at wavelengths longer than 700 nm. The ability of the window to modulate near-infrared light is important for the modulation of heat flux into buildings. Photographs (Fig. 8b–8d) of the device during tinting demonstrate uniform switching

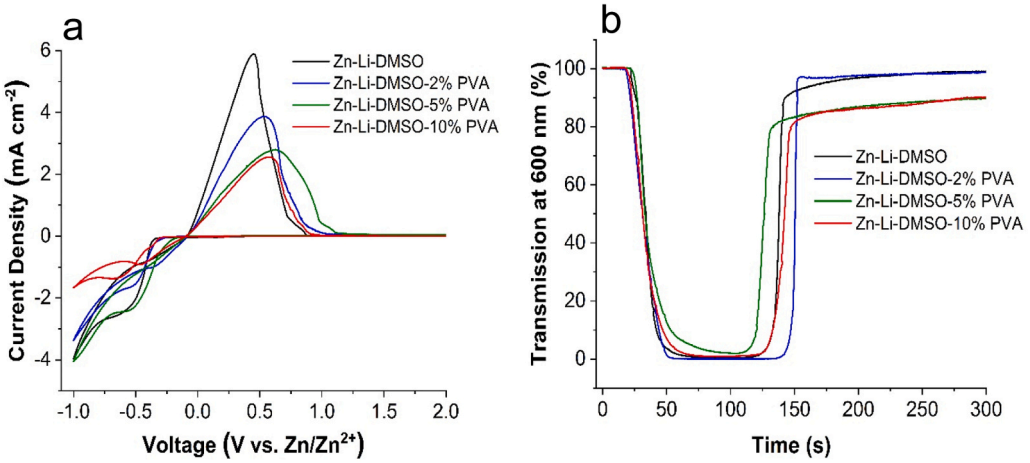

Fig. 7. Effect of PVA Concentration on Spectroelectrochemistry of Pt-Modified ITO Electrodes in Li-ZnDMSO Electrolytes. Cyclic voltammograms (a) and corresponding transmission at 600 nm (b) of Pt-modified ITO electrodes at a scan rate of 20 mV s^{-1} in DMSO electrolytes containing 300 mM $ZnBr_2$, 200 mM $LiCF_3COO$, 400 mM LiCOOH (Li-ZnDMSO) without PVA (black line), with 2 wt% PVA (blue line), with 5 wt% PVA (green line), or 10 wt% PVA (red line).

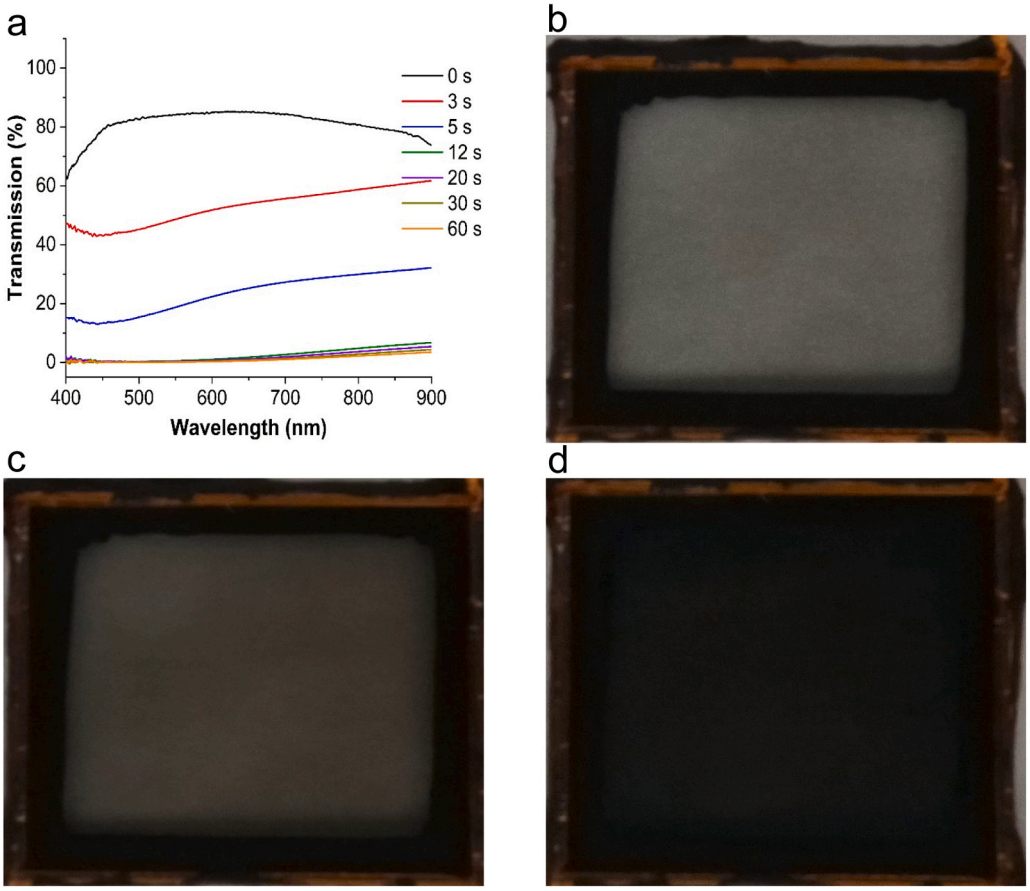

Fig. 8. Zn Dynamic Window at Various Tinting Times. Transmission (a) of a two-electrode 25 cm^2 Zn dynamic window using a DMSO electrolyte containing 300 mM $ZnBr_2$, 200 mM $LiCF_3COO$, 400 mM LiCOOH, and 2 wt% PVA after tinting at −0.9 V for 0 s (black line), 3 s (red line), 5 s (blue line), 12 s (green line), 20 s (purple line), 30 s (yellow line), and 60 s (orange line). Photographs of the same device after 0 s (b), 5 s (c), and 12 s (d) of Zn electrodeposition.

at this scale. We have previously thoroughly modeled and discussed considerations regarding larger dynamic windows utilizing a Zn DMSO electrolyte [13] and hence work aimed at demonstrating large RME windows is outside the scope of this manuscript.

Long-term cycleability is a paramount challenge hindering the implementation of all dynamic window technologies. Recently, we demonstrated that RME windows with an acetate-based Zn DMSO electrolyte can cycle 10,000 times with a relatively stable contrast ratio and a lower transmission value of 30% [14]. To achieve 10,000 cycles, we progressively increased the magnitude of the electrodeposition voltage to counteract electrolyte degradation and maintain a constant switching speed.

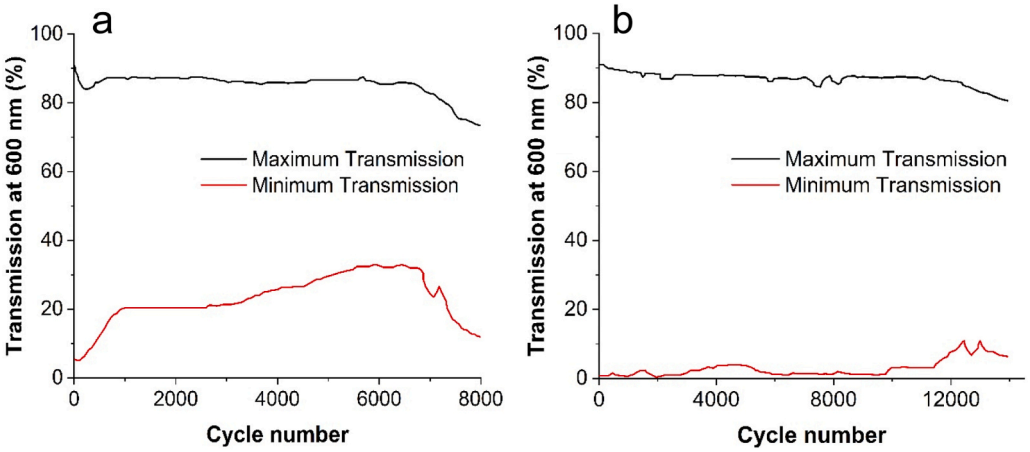

Fig. 9. Cycling Performance of Zn Dynamic Windows. Maxima (black line) and minima (red line) transmission at 600 nm of a two-electrode 25 cm^2 Zn dynamic window during 8000 switching cycles with a DMSO electrolyte containing 300 mM $ZnBr_2$, 300 mM $Zn(CH_3COO)_2$, 400 mM $NaCH_3COO$, and 2 wt% PVA using −0.9 V for 30 s for device darkening and +1.0 V for 60 s for device lightening. Maxima (black line) and minima (red line) transmission at 600 nm of a two-electrode 25 cm^2 Zn dynamic window during 14,000 switching cycles with a DMSO electrolyte containing 300 mM $ZnBr_2$, 200 mM $LiCF_3COO$, 400 mM LiCOOH, and 2 wt% PVA using −0.9 V for 12 s for device darkening and +1.0 V for 50 s for device lightening.

In this manuscript, we cycled a dynamic window with the same previously reported acetate-based Zn DMSO electrolyte but held the switching parameters constant (-0.9 V for 30 s for darkening and +1.0 V for 60 s for lightening). Under these conditions, the minimum attained transmission during each cycle slowly increases during cycling (Fig. 9A), resulting in a diminished contrast ratio of the device. By comparison, a window utilizing the new Li-ZnDMSO developed in this work exhibits superior cycling characteristics. First, with a darkening time of only 12 s at −0.9 V (compared to 30 s for the previously reported acetate-based Zn DMSO electrolyte) and a lightening time of only 50 s at +1.0 V, the Li-Zn DMSO device cycles reversibly to a ~1% dark state (Fig. 9B). This ~1% dark state is much more opaque than the >5% dark state achieved by the device with the acetate electrolyte (Fig. 9A) and cycling to more opaque dark states is known to accelerate device degradation in a manner similar to the deep cycling of batteries [30]. Despite the darker cycling of the Li-Zn DMSO device, the window cycles more than 11,000 times with a relatively steady contrast ratio (Fig. 9B), far exceeding the performance of the acetate-based device. To the best of our knowledge, the cycling performance of the Li-ZnDMSO window (deep cycling at >10,000 cycles) presented here is entirely unprecedented in the RME window literature. This result represents an important milestone in the quest for RME windows to achieve the 50,000 cycles stipulated by ASTM standards [16].

To understand the enhanced cycle life of a device using the Li-ZnDMSO electrolyte, we conducted SEM imaging of the Zn electrodeposits as a function of cycle number. The initial morphology of the Zn electrodeposits (Fig. 2, b and b') is very similar to the morphologies observed after 500 cycles (Fig. 10, a and a') and 5000 cycles (Fig. 10, b and b'), suggesting that the Zn RME process is highly reversible over the first 5000 cycles. After 8000 cycles (Fig. 10, c and c') and 14,000 cycles (Fig. 10, d and d'), the coarseness of the electrodeposits progressively increases and this nonuniformity likely causes the electrodeposits to block light less efficiently, thereby diminishing switching speed. Indeed, the charge density required to reach 10% transmission progressively increases during cycling, which is consistent with coarser electrodeposits (Fig. S5a). The tinting time required to reach 10% transmission also correspondingly increases (Fig. S5b), indicating that the switching speed of the device slowly decreases during cycling. The clear-state transmission of the device also slowly decreases during cycling. This trend has been observed previously in RME window cycling and is attributed to residual metal that remains on the electrode surface despite extensive electrochemical stripping [9]. In future work, we will study the use of more complicated voltage profiles to more explicitly control metal nucleation and growth over tens of thousands of cycles to further improve device cyclability.

3. Conclusions

This manuscript illuminates the critical role electrolyte design plays in facilitating reversible Zn electrodeposition in DMSO electrolytes. Systematic studies reveal the role of anions, cations, and PVA on the electrochemical and optical performance of the Zn electrolytes. The optimized Li-ZnDMSO electrolyte exhibits a high Coulombic efficiency of 99.5% and enables practical two-electrode 25 cm^2 dynamic windows to switch to a dark opaque state of ~1% transmission at 600 nm within 12 s. Impressively, the device switches 14,000 times at a constant switching speed and voltage profile, while maintaining a relatively constant optical contrast ratio. Taken together, RME windows utilizing the developed Li-ZnDMSO electrolyte represent a significant step forward towards achieving practical metal-based dynamic windows that pass ASTM-E2141 standards for the first time.

4. Materials and methods

4.1. Chemicals

Chemicals used in this study were procured from commercial suppliers and employed without additional purification. Anhydrous DMSO was obtained from DMSO Store, Inc. $NaCH_3COO$ (99.99%), $LiCH_3COO$ (99%), NaCOOH (99%), LiCl (99%), LiBr (99%), LiF (99%), $LiPF_6$ (99%), $LiClO_4$ (97%), and $LiCF_3SO_3$ (99.95%) were acquired from Oakwood Chemical. $Zn(CH_3COO)_2$ (99.99%) originated from ProChem,

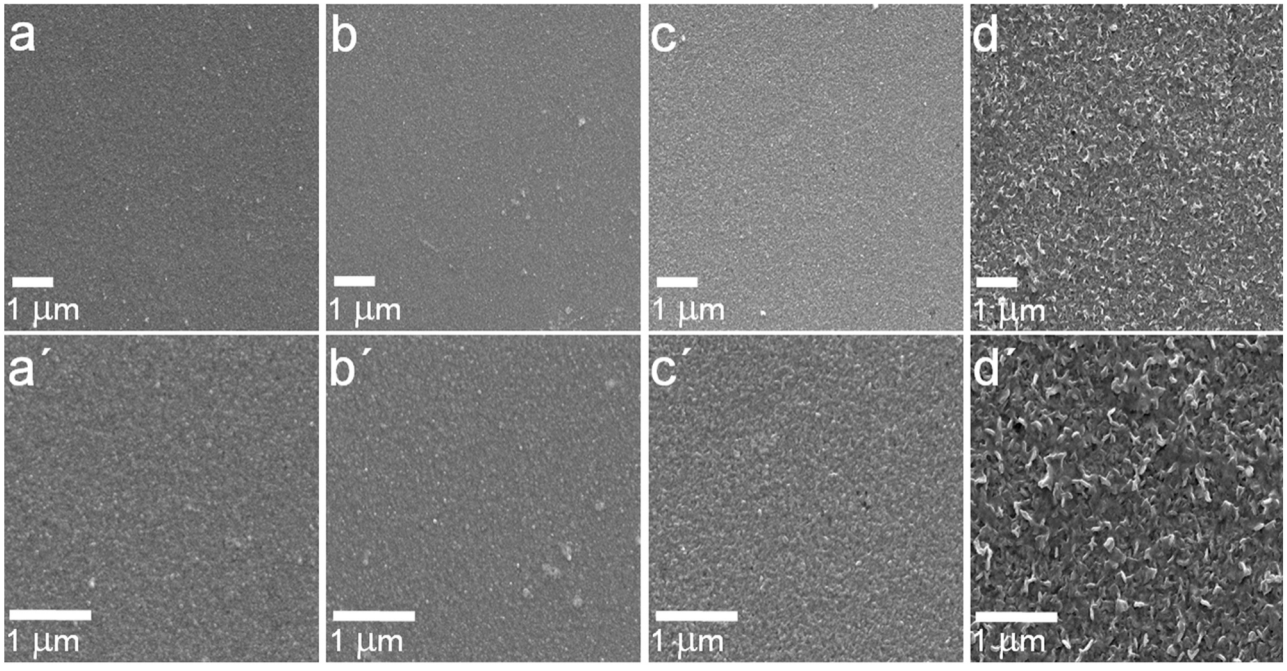

Fig. 10. Influence of Cycling on Zn Electrodeposit Morphology in Dynamic Windows. Scanning electron micrographs of Zn electrodeposits produced from Li-ZnDMSO electrolytes containing 300 mM $ZnBr_2$, 200 mM CF_3CO_2Li, 400 mM HCO_2Li, and 2 wt% PVA using chronoamperometry at −0.9 V until the electrode transmission is equal to 5% after 500 cycles (a, a′, two different magnifications), 5000 cycles (b, b′, two different magnifications), 8000 cycles (c, c′, two different magnifications), or 14,000 cycles (d, d′, two different magnifications) in a 25 cm^2 dynamic window using the parameters described in Fig. 9.

Inc., and $ZnBr_2$ (99.999%) was purchased from Alfa Aesar. KCOOH (99%), LiCOOH (98%), and $LiCF_3COO$ (97%) were acquired from Thermo Scientific Chemicals. LiI (99.9%) and PVA with a molecular weight range of 31,000–50,000 were purchased from Sigma Aldrich. Moreover, $NaCF_3COO$ (98%) was procured from TCI America, Inc. ITO on glass substrates (15 Ω/sq) were sourced from Xin Yan, Inc. Additionally, an aqueous dispersion of Pt nanoparticles (3 nm in diameter, 1000 ppm) was procured from US Research Nanomaterials, Inc.

4.2. Experimental procedures

For three-electrode experiments, we used a Zn metal foil (99.9%) as the reference electrode and another Zn metal foil as the counter electrode. The modification of ITO on glass involved spraying a 3:1 vol% dispersion of water and Pt nanoparticles. The resulting Pt-modified ITO on glass substrates were heated under air at 200 °C for 20 minutes and used as working electrodes. The Pt nanoparticles act as a seed layer, improving metal nucleation kinetics and electrodeposit uniformity, as mentioned in previous studies [4,22,23]. Electrochemistry was conducted using a VSP-300 Biologic potentiostat. All CV data presented are from the second cycle. Transmission data were recorded with an Ocean Optics FLAME-S-VIS-NIR spectrometer combined with an Ocean Insight HL2000-FHSA light source. Viscosities were Viscosities were determined using a NDJ-5S viscometer. We determined electrolyte ionic conductivity from solution resistance as measured by electrochemical impedance spectroscopy (EIS) using standard protocols [31]. The frequency range utilized was from 10^5 to 0.1 Hz with an amplitude of 15 mV. Data points were collected at a rate of five points per decade. The potential was maintained at 0 V with respect to open circuit potential. The datum point at 10 kHz was selected for resistance determination, which was then normalized to the area and thickness of the sample.

For three-electrode spectroelectrochemical experiments, measurements were made in a 2 cm × 2 cm glass cuvette with 5 mL of electrolyte. A transmission value of 100% was defined with the cuvette containing only the electrolyte, excluding the working electrode. Solutions were prepared by adding the appropriate solids to 20 mL of deionized water. For electrolytes with PVA, 2 wt% PVA was then added, and the mixture was stirred overnight at 60 °C. The samples were cooled to room temperature before experimental analysis.

For two-electrode 25 cm^2 dynamic windows, Cu tape with conductive adhesive was applied along the edges of the Pt-modified ITO on glass to make uniform electrical connection to the working electrode perimeter. Zn counter electrode meshes were fabricated from commercially available Cu mesh (TWP, Inc.) as described previously [14]. In short, Zn was electrodeposited onto the Cu mesh using a Ni strike to improve Zn adhesion and uniformity. This mesh was placed on top of a nonconductive glass backing. Butyl rubber (Solargain, Quanex, Inc.) sealed the two electrodes together with an interelectrode spacing of about 5 mm. Gel electrolyte injection into the device stacked through the butyl rubber sealant was done using a syringe. The outside surfaces of the completed dynamic window were cleaned with glass cleaner before optical measurements. For window experiments, a transmission value of 100% represented open air.

4.3. Materials characterization

Electrochemical assessments were conducted employing a VSP-300 Biologic potentiostat within a 2 cm×2 cm glass cube cuvette. A potential of −0.9 V vs. Zn/Zn^{2+} was applied consistently in all chronoamperometry tests, utilizing distinct Zn metal counter and reference electrodes, along with a Pt-coated ITO on a glass working electrode. Transmission measurements were executed using a halogen light source and a spectrometer from Ocean Optics (Flame). Scanning electron microscope (SEM) images were obtained using a JOEL JSM-6010LA microscope with an operating voltage of 20 kV.

CRediT authorship contribution statement

Christopher J. Barile: Writing – review & editing, Writing – original draft, Project administration, Methodology, Funding acquisition, Formal analysis, Conceptualization. **Samantha M. Thompson:** Writing – review & editing, Investigation. **Nikhil C. Bhoumik:** Writing – original draft, Writing - review & editing Methodology, Investigation, Formal analysis, Data curation.

Declaration of Competing Interest

The authors declare the following financial interests/personal relationships which may be considered as potential competing interests: Christopher Barile reports a relationship with Tynt Technology that includes: consulting or advisory. Christopher Barile has patent pending to USPTO. Nikhil Bhoumik has patent pending to USPTO. If there are other authors, they declare that they have no known competing financial interests or personal relationships that could have appeared to influence the work reported in this paper.

Data Availability

Data will be made available on request.

Acknowledgements

This material is based upon work supported by the National Science Foundation Award under Grant No. ECCS2127308. SEM-EDX analysis was done in the Mackay Microbeam Laboratory at UNR, and we acknowledge J. Desormeau for his kind assistance.

Appendix A. Supporting information

Supplementary data associated with this article can be found in the online version at doi:10.1016/j.nanoen.2024.109710.

References

[1] Monthly Energy Review. July 2020, U.S. Energy Information Administration, ⟨https://www.eia.gov/totalenergy/data/monthly/archive/00352007.pdf⟩ / (accessed: January 2021).
[2] E. Lee, M. Yazdanian, S. Selkowitz, The Energy-savings Potential of Electrochromic Windows in the US Commercial Buildings Sector, 2019, ⟨https://www.osti.gov/servlets/purl/891618/⟩ (accessed: January 5, 2021).
[3] R. Tällberg, B.P. Jelle, R. Loonen, T. Gao, M. Hamdy, Comparison of the energy saving potential of adaptive and controllable smart windows: a state-of-the-art review and simulation studies of thermochromic, photochromic and electrochromic technologies, Sol. Energ. Mat. Sol. C 200 (2019) 109828, https://doi.org/10.1016/j.solmat.2019.02.041.
[4] S.M. Islam, C.J. Barile, Dynamic windows using reversible zinc electrodeposition in neutral electrolytes with high opacity and excellent resting stability, Adv. Energy Mater. 11 (2021) 2100417, https://doi.org/10.1002/aenm.202100417.
[5] R.J. Mortimer, A.L. Dyer, J.R. Reynolds, Electrochromic organic and polymeric materials for display applications, Displays 27 (2006) 2–18, https://doi.org/10.1016/j.displa.2005.03.003.
[6] Y. Liu, X. Zhu, M. Yuan, X. Jiang, X. Tang, A. Xu, Y. Wang, L. Yuan, Y. Duan, Silver reversible electrodeposition device under −40 °C condition, Appl. Phys. Lett. 123 (2023), https://doi.org/10.1063/5.0187109.
[7] E.L. Runnerstrom, A. Llordés, S.D. Lounis, D.J. Milliron, Chem. Commun. 50 (2014) 10555, https://doi.org/10.1039/c4cc03109a.
[8] E. Alice Lee Sie, Thesis, Nanyang Technological University, 2020.
[9] C.J. Barile, D.J. Slotcavage, J. Hou, M.T. Strand, T.S. Hernandez, M.D. McGehee, Dynamic windows with neutral color, high contrast, and excellent durability using reversible metal electrodeposition, Joule 1 (2017) 133–145, https://doi.org/10.1016/j.joule.2017.06.001.
[10] T.S. Hernandez, C.J. Barile, M.T. Strand, T.E. Dayrit, D.J. Slotcavage, M. D. Mcgehee, Bistable black electrochromic windows based on the reversible metal electrodeposition of Bi and Cu, ACS Energy Lett. 3 (2018) 104–111, https://doi.org/10.1021/acsenergylett.7b01072.
[11] S.M. Islam, C.N. Fini, C.J. Barile, Dynamic windows based on reversible metal electrodeposition with enhanced functionality, J. Electrochem. Soc. 166 (2019) D333–D338, https://doi.org/10.1149/2.0961908jes.

[12] C.W. Moon, Y. Kim, J.K. Hyun, Active electrochemical high-contrast gratings as on/off switchable and color tunable pixels, Nat. Commun. 13 (2022) 3391, https://doi.org/10.1038/s41467-022-31083-z.
[13] D.C. Madu, S.M. Islam, H. Pan, C.J. Barile, Electrolytes for reversible zinc electrodeposition for dynamic windows, J. Mater. Chem. C 9 (2021) 6297–6307, https://doi.org/10.1039/D1TC00857A.
[14] N.C. Bhoumik, D.C. Madu, C.W. Moon, L.S. Arvisu, M.D. McGehee, C.J. Barile, Nonaqueous electrolytes for reversible zinc electrodeposition for dynamic windows with excellent optical contrast and durability, Joule 8 (2024) 1036–1049, https://doi.org/10.1016/j.joule.2024.01.023.
[15] J.N. Butler, Electrochemistry in dimethyl sulfoxide, J. Electroanal. Chem. Interfacial Electrochem. 14 (1967) 89–116, https://doi.org/10.1016/0022-0728(67)80136-0.
[16] ASTM Stand News 2014, 12, E2141-14. Standard Test Method for Accelerated Aging of Electrochromic Devices in Sealed Insulating Glass Units.
[17] D.C. Madu, M.V. Lilo, A.A. Thompson, H. Pan, M.D. Mcgehee, C.J. Barile, Investigating formate, sulfate, and halide anions in reversible zinc electrodeposition dynamic windows, ACS Appl. Mater. Inter. 14 (2022) 47810–47821, https://doi.org/10.1021/acsami.2c14893.
[18] W.M. Haynes, CRC Handbook of Chemistry and Physics, 97th Edition, Vol. 3, Ringgold, Inc, Beaverton 2016.
[19] R.M. Smith, A.E. Martell, Critical Stability Constants: Second Supplement, Vol. 6, Springer, 1989.
[20] R.N. Goldberg, N. Kishore, R.M. Lennen, Thermodynamic quantities for the ionization reactions of buffers, J. Phys. Chem. Ref. Data 31 (2002) 231–370.
[21] A.J. Bard, L.R. Faulkner, H.S. White, Electrochemical Methods: Fundamentals and Applications, John Wiley & Sons, 2022.
[22] M.T. Strand, T.S. Hernandez, M.G. Danner, A.L. Yeang, N. Jarvey, C.J. Barile, M. D. McGehee, Polymer inhibitors enable >900 cm2 dynamic windows based on reversible metal electrodeposition with high solar modulation, Nat. Energy 6 (2021) 546–554, https://doi.org/10.1038/s41560-021-00816-7.
[23] M.T. Strand, C.J. Barile, T.S. Hernandez, T.E. Dayrit, L. Bertoluzzi, D.J. Slotcavage, M.D. McGehee, Factors that determine the length scale for uniform tinting in dynamic windows based on reversible metal electrodeposition, ACS Energy Lett. 3 (2018) 2823–2828, https://doi.org/10.1021/acsenergylett.8b01781.
[24] C.W. Moon, N.C. Bhoumik, P. Mondol, S.H. Park, H.W. Jang, C.J. Barile, Origin of high optical contrast in zinc-zinc oxide electrodeposits for dynamic windows, Nano Energy 114 (2023) 108666, https://doi.org/10.3390/mi15030334.
[25] H. Kim, B.K. Kang, C.W. Moon, Refractive index modulation for metal electrodeposition-based active smart window applications, Micromachines 15 (2024) 334, https://doi.org/10.3390/mi15030334.
[26] K. Kondo, H. Kouta, M. Yokoi, N. Okamoto, T. Saito, T. Hayashi, Cuprous ion as an accelerant of copper damascene electrodeposition, ECS Trans. 58 (2014) 89–96.
[27] M. Schlesinger, Modern Electroplating, Wiley, 2010.
[28] J. Malathi, M. Kumaravadivel, G. Brahmanandhan, M. Hema, R. Baskaran, S. Selvasekarapandian, Structural, thermal and electrical properties of PVA–LiCF3SO3 polymer electrolyte, J. Non-Cryst. Solids 356 (2010) 2277–2281.
[29] Q. Zhang, Q. Li, D. Liu, X. Zhang, X. Lang, J. Mol. Liq. (2018) 249, 1097.
[30] W. Diao, J. Kim, M.H. Azarian, M. Pecht, Degradation modes and mechanisms analysis of lithium-ion batteries with knee points, Electrochim. Acta 431 (2022) 141143.
[31] S. Wang, J. Zhang, O. Gharbi, V. Vivier, M. Gao, M.E. Orazem, Electrochemical impedance spectroscopy, Nat. Rev. Methods Prim. 1 (2021) 41.

Nikhil Chandra Bhoumik is an accomplished researcher in the field of electrochemistry. He holds Master's and M.Phil. Degrees in Physical Inorganic and Organometallic Chemistry, respectively, from Jahangirnagar University, Bangladesh. In 2021, he commenced his Ph.D. studies in the Department of Chemistry at the University of Nevada, Reno, USA. Currently, his research focuses on developing innovative electrolytes and electrodes to enable reversible metal electrodeposition, thereby enhancing energy efficiency in various applications, including dynamic windows and battery industries. Additionally, he possesses substantial expertise in single crystal X-ray crystallography, particularly within the field of organometallic chemistry.

Samantha Thompson is an undergraduate student at the University of Nevada, Reno pursuing a bachelor's in chemical engineering with a biomedical emphasis and mathematics minor. Her primary research interests are electrochemical and focus on the application of unique metal and electrolyte compositions in dynamic window construction. Previous research included utilizing mathematical modeling for early identification of scoliosis based on X-ray and epidermal imaging.

Christopher J. Barile is the Clemons-Magee Professor in the chemistry department at the University of Nevada, Reno. Prof. Barile earned a BSc. with distinction and co-terminal MSc. degrees in chemistry from Stanford University. He then attended the University of Illinois at Urbana-Champaign and earned his PhD focusing on the development of next-generation battery technologies. Prof. Barile subsequently returned to Stanford as a postdoctoral scholar in materials science and engineering before launching his independent career in 2017. His research lies at the intersection of electrochemistry, inorganic chemistry, and materials chemistry with an emphasis on solving problems associated with energy conversion, storage, and efficiency.